Facile Synthesis of Bi₂S₃@SiO₂ Core-Shell Microwires as High-Performance Anode Materials for Lithium-Ion Batteries

Chunjuan Tang,[a,b,=] **Narui Li,**[a,=] **Jinzhi Sheng,**[a] **Liang Zhou,**[a,z] **Liang He,**[a] **Jiexin Zhu,**[a] **Feng Li,**[a] **Yuning Liu,**[a] **and Liqiang Mai**[a,z]

[a]*State Key Laboratory of Advanced Technology for Materials Synthesis and Processing, Wuhan University of Technology, Wuhan 430070, Hubei, People's Republic of China*
[b]*Department of Mathematics and Physics, Luoyang Institute of Science and Technology, Luoyang 471023, People's Republic of China*

Anode materials with high capacity are urgently required to substitute graphite. The theoretical gravimetric and volumetric capacities of Bi₂S₃ are much higher than those of graphite, but the cycling performance of Bi₂S₃ is poor due to its large volumetric expansion. Amorphous SiO₂ is mechanically rigid, which can buffer the volume change. A novel Bi₂S₃@SiO₂ core-shell microwire is firstly designed and synthesized in this work. The composite exhibits excellent electrochemical performances. The discharge capacity is 379 mA h g⁻¹ after 4000 cycles at the current density of 1 A g⁻¹.

The depletion of fossil fuels and the pollution of environment are two major issues to our society. The development of renewable energy and new energy storage technologies is a promising way to solve these problems. As a widely used energy storage technology, lithium ion batteries (LIBs) have high energy density and environmental benignity.[1,3] However, the low theoretical capacity of graphite limits the further application of LIBs in electric vehicles. In this regard, alternative anode materials with higher capacity have been developed, such as Si,[4] Sn,[5] metal oxides,[6] and metal sulfides.[7]

As a typical metal sulfide, Bi₂S₃ has been widely used in many fields, such as optics,[8,9] photoelectricity,[10,11] photocatalysis,[12,13] and biology.[14,15] Due to its lamellar structure, Bi₂S₃ is also investigated as an ideal host for hydrogen[16,17] and lithium storage.[18,19] As an anode material for LIBs, Bi₂S₃ can afford the theoretical capacities of 625 mA h g⁻¹ by mass and 4250 mA h cm⁻³ by volume, which is much higher than that of graphite. Although Bi₂S₃ has many advantages, such as high capacity, nontoxic, and low cost, its practical application is hindered by the poor cycling stability due to its large volumetric expansion.[15] According to the reaction mechanism proposed by Jung et al., the Li⁺ storage of Bi₂S₃ involves conversion (Bi₂S₃ + 6 Li⁺ + 6 e⁻ ↔ 2 Bi + 3 Li₂S) and alloying processes (Bi + 3 Li⁺ + 3 e⁻ ↔ Li₃Bi).[20] The conversion step causes a volume expansion of 90%, the alloying results in a volume increase of 113%, and the total volume expansion is 164%.[19] Such a huge volume variation during charge-discharge process leads to severe pulverization of the Bi₂S₃, resulting in a rapid capacity fading. It has been reported that hierarchical nanostructures can provide higher surface to volume ratios and accommodate the volume change.[21,24] As a result, various Bi₂S₃ based hierarchical nanostructures, such as nanomeshes and microspheres have been synthesized.[19,25] However, the capacity retention is still unsatisfactory. Combining active materials with carbonaceous matrix is another way to accommodate the volume expansion during charge-discharge process.[19,26,29] Ni et al. synthesized Bi₂S₃@CNT composite, which shows excellent electrochemical performance. It delivers a capacity of 405 mA h g⁻¹ at 1 A g⁻¹ after 100 cycles.[29] Besides carbonaceous materials, metal oxides, such as ZrO₂ and SiO₂, are also used as the coating layer to suppress the volume expansion and improve the cycling stability of electrode materials.[30,34]

In this work, SiO₂ is selected as the coating layer due to its low cost and simple synthesis method. A novel Bi₂S₃@SiO₂ core-shell microwire structure is designed to improve the cycling performance of Bi₂S₃ (Fig. 1). The mechanically rigid SiO₂ can suppress the volume expansion of Bi₂S₃, allow the lithium ions to penetrate through, and form an efficient barrier to prevent the direct contact of Bi₂S₃ with the electrolyte.[31,34] As a result, the cycling stability can be significantly enhanced. The as-obtained Bi₂S₃@SiO₂ composite delivers a capacity of 553 mA h g⁻¹ after 100 cycles at 0.2 A g⁻¹ and 379 mA h g⁻¹ after 4000 cycles at 1 A g⁻¹.

Experimental

Synthesis.—All the reagents used in the experiment are of analytical grade and used without further purification. Bi₂S₃ microwires are synthesized according to the literature.[35] Bi(NO₃)₃ · 5H₂O (4 mmol) was dissolved into 54 mL glycerol at 60°C. NaOH (0.162 mol) was put into 27 mL deionized water with stirring. When the solutions cooled to room temperature naturally, they were mixed together and stirred for 10 min. Then, Na₂S₂O₃ (12.7 mmol) was dissolved into the mixture and stirred for another 10 min. Finally, the solution was transferred into an autoclave. The autoclave was maintained at 180°C for 24 h. The products floated on the top of the solution was collected, washed with deionized water and ethanol for ten times and dried at 60°C for 8 h. 5 mmol Bi₂S₃ microwires was suspended into the solution of 80 mL ethanol and 20 mL deionized water under ultrasonication for 1 h, then 1 mL ammonia was added into the solution. Tetraethyl silicate (0.4 mL) was added into the solution drop by drop and stirred for 1 h. The product was washed with deionized water and ethanol for six times and dried at 60°C for 4 h.

Materials characterization.—X-ray diffraction (XRD) was carried out on a D8 Advanced X-ray diffractometer with a non-monochromated Cu Kα X-ray source. The morphology and microstructure of the samples were characterized by field emission scanning electron microscopy (SEM, JEOL-7100F), transmission electron microscopy (TEM), and high resolution TEM (HRTEM, JEM-2100F STEM/EDS) associated with selected area electron diffraction (SAED).

Electrochemical characterization.—The slurry of the sample was prepared with 75 wt% active material, 20 wt% acetylene black conductive additive, and 5 wt% carboxyl methyl cellulose (CMC) binder.

=These authors contributed equally to this work.
zE-mail: liangzhou@whut.edu.cn; mlq518@whut.edu.cn
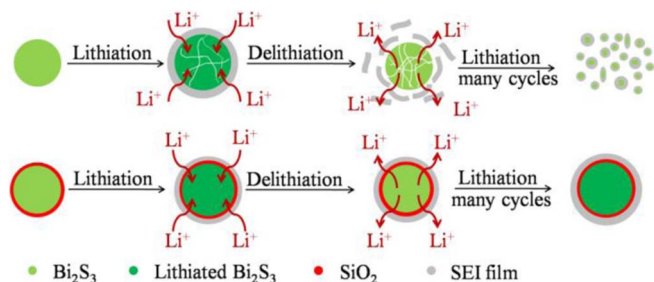
Figure 1. Schemetic illustration of silica coating stablizes the structure of Bi_2S_3.

The CMC was dispersed into distilled water under ultrasonication for 1 h. Then the mixture of active material and conductive additive was manually ground for 15 min and dispersed in the CMC suspension via ultrasonication for 1 h. The slurry was pasted on copper foil, dried at 70°C for 2 h and then dried at 120°C for 24 h in a vacuum oven. The copper foil was cut into round pieces. Electrolyte was the mixture of ethylene carbonate and dimethyl carbonate (50/50, v/v) containing 1.0 M lithium hexafluorophosphate ($LiPF_6$). The electrochemical performances were characterized by assembling coin-type cell CR2016 with lithium metal foil as counter and reference electrode. Galvanostatic discharge-charge measurements were conducted in a potential range of 0.01–3 V vs. Li^+/Li (LAND CT2001A). Cyclic voltammetry (CV) and electrochemical impedance spectroscopy (EIS) were performed by electrochemical workstation (Autolab Potentiostat Galvanostat 302N and CHI760D). All of the measurements were carried out at room temperature.

Results and Discussion

XRD patterns of the products are shown in Fig. 2. All the diffraction peaks of Bi_2S_3 and $Bi_2S_3@SiO_2$ can be well indexed to orthorhombic Bi_2S_3 phase (JCPDS No. 00-043-1471). It can be seen clearly that there are no impurities in the products. The XRD pattern of $Bi_2S_3@SiO_2$ is almost the same with that of Bi_2S_3, except for the slight weakness in peak intensity.

The morphology of the products was characterized by SEM and TEM. It can be seen from Fig. 3a that $Bi_2S_3@SiO_2$ shows microwire morphology with millimeter length. The diameters of the microwires are not so uniform and range from tens to hundreds nanometers. The SiO_2 coating layer on Bi_2S_3 can be observed clearly in high-magnification SEM image (Fig. 3b). Fig. 3c presents the energy dispersive X-ray spectroscopic (EDS) elemental mapping results of the
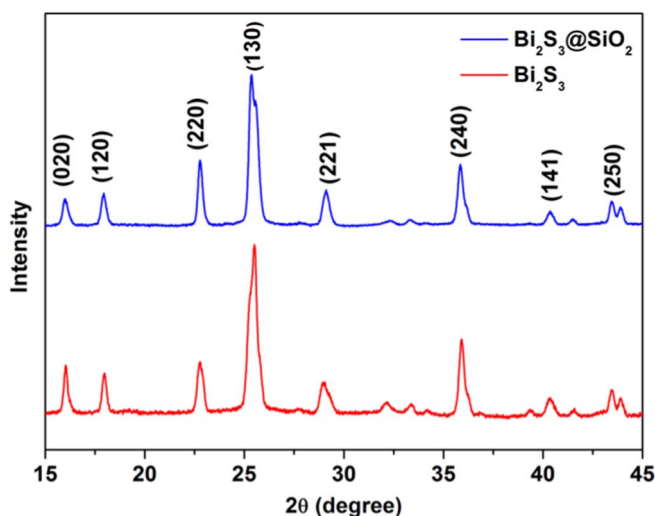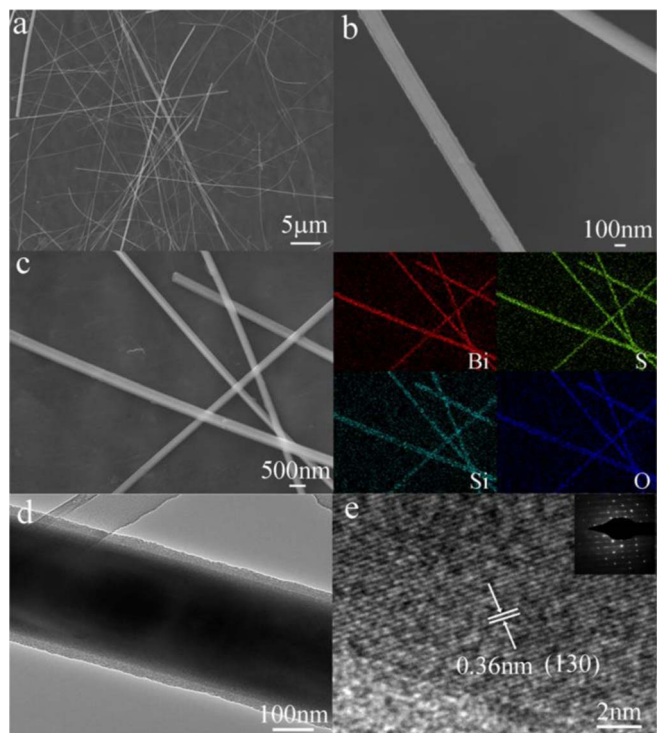

Figure 3. SEM images of $Bi_2S_3@SiO_2$ (a, b), EDS elemental mapping of $Bi_2S_3@SiO_2$ (c), TEM image of an individual $Bi_2S_3@SiO_2$ microwire (d), HRTEM image of the $Bi_2S_3@SiO_2$ microwire (e). The inset is the corresponding SAED pattern.

$Bi_2S_3@SiO_2$ microwires. The Bi, S, Si, and O are uniformly distributed in the composite, further indicating that Bi_2S_3 microwires are coated with a SiO_2 layer. TEM image of the $Bi_2S_3@SiO_2$ microwire shows the obvious core-shell structure (Fig. 3d). The thickness of the SiO_2 coating layer is determined to be 16 nm. The HRTEM image presented in Fig. 3e shows clear interplaner distance of 0.36 nm, corresponding to the (130) lattice fringes of orthorhombic Bi_2S_3. The SAED pattern (Fig. 3e inset) indicates that the Bi_2S_3 microwires are generally single crystalline.

The electrochemical performances of $Bi_2S_3@SiO_2$ microwires and Bi_2S_3 microwires are further characterized. Cyclic voltammogram (CV) curves of $Bi_2S_3@SiO_2$ microwires are shown in Fig. 4a. The peak at about 1.64 V in the first cathodic scan is ascribed to the decomposition of Bi_2S_3 into Li_2S and metallic Bi. The peaks centered at 0.74 and 0.62 V correspond to the formation of LiBi and Li_3Bi alloys.[20] In the first anodic process, there is a sharp peak at 0.95 V, which is ascribed to the dealloying of Li_3Bi to Bi. The weak peaks at 2.13 and 2.36 V are attributed to the formation of Bi_2S_3.[19,20] The subsequent CV curves generally overlap with the first one except for the cathodic peak at 1.64 V, suggesting the excellent Li-storage reversibility. The CV curves of Bi_2S_3 microwires shown in Fig. 4b are similar with those of the $Bi_2S_3@SiO_2$ composite.

Fig. 4c shows the representative discharge-charge curves of $Bi_2S_3@SiO_2$ at the current density of 0.2 A g^{-1}. There are two flat plateaus at around 1.6 and 0.7 V in the first discharge process, and a significant flat plateau from 0.9 V to 1 V is observed in the following charge process, which is in accordance with the peaks of CV curve. For the following discharge-charge curves, the curves are almost the same with each other except that the plateau at 1.6 V becomes less distinct. The $Bi_2S_3@SiO_2$ composite delivers initial discharge and charge capacities of 973 and 718 mA h g^{-1}, respectively. And the corresponding coulombic efficiency is 73.8%. Representative discharge-charge curves of bare Bi_2S_3 microwires are shown in Fig. 4d. Compared to the $Bi_2S_3@SiO_2$ core-shell microwires, the bare Bi_2S_3 microwires show much quicker capacity decay.

Figure 2. XRD patterns of the products.
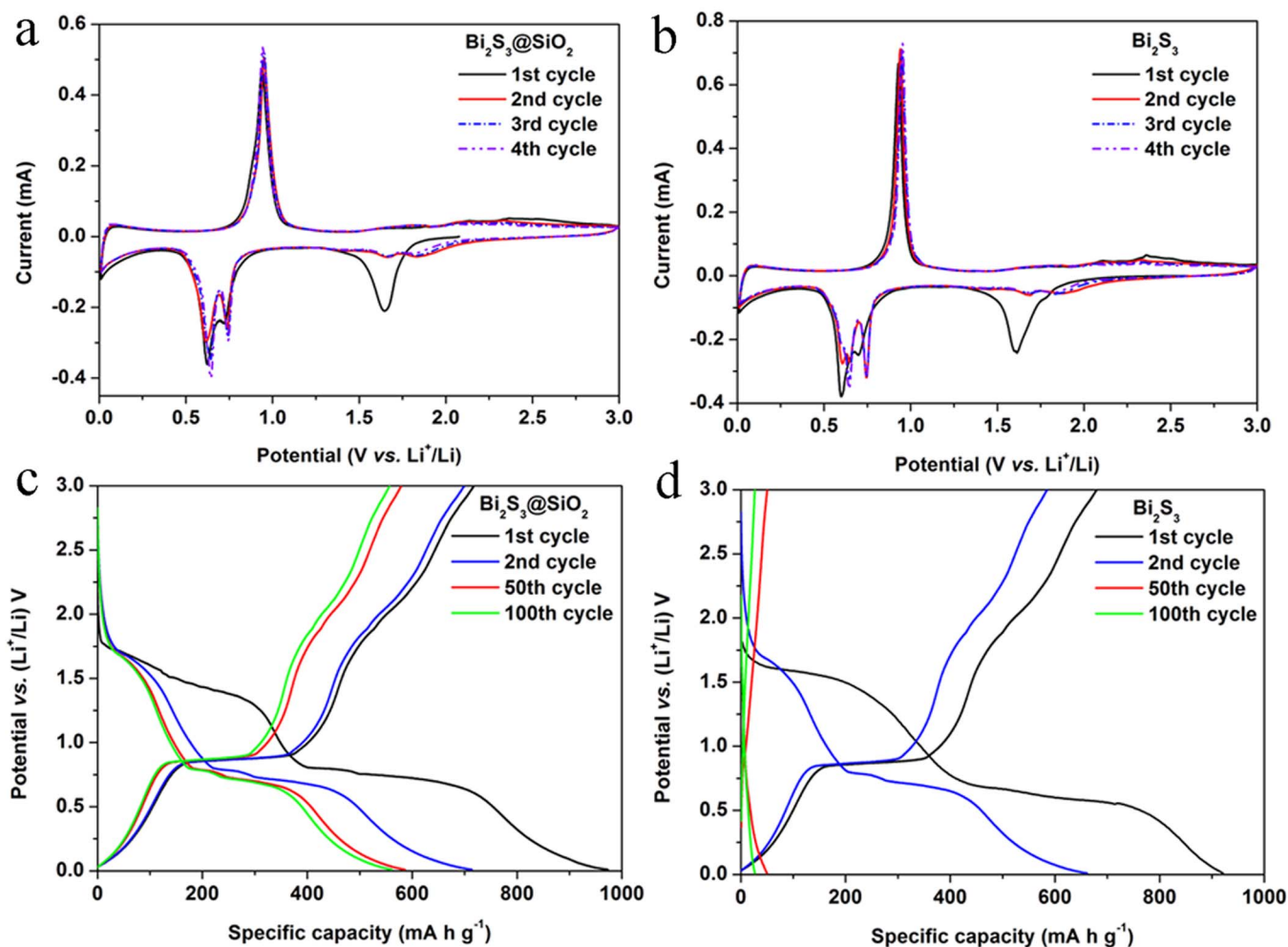
Figure 4. CV curves of $Bi_2S_3@SiO_2$ microwires (a) and Bi_2S_3 microwires (b) at a scan rate of 0.2 mV s^{-1} in the potential range from 3.0 to 0.01 V vs. Li$^+$/Li, discharge-charge curves of $Bi_2S_3@SiO_2$ microwires (c) and Bi_2S_3 microwires (d) at a current density of 0.2 A g^{-1}.

Fig. 5a displays the galvanostatic cycling performance of the $Bi_2S_3@SiO_2$ composite and bare Bi_2S_3. Both samples exhibit a large irreversible capacity at initial stage, which may be ascribed to the formation of solid electrolyte interphase (SEI) layer on the electrode surface. The $Bi_2S_3@SiO_2$ composite exhibits a slight capacity fading in the first 20 cycles and a stable capacity of around 600 mA h g^{-1} afterwards. Even after 100 cycles at 0.2 A g^{-1}, a capacity of 553 mA h g^{-1} can be maintained, which is much higher than that of bare Bi_2S_3 microwires (277 mA h g^{-1}). The rate performances of the samples are shown in Fig. 5b (from the second cycle). The $Bi_2S_3@SiO_2$ composite displays excellent rate capability and it delivers capacities of 787, 585, 512, 411, 315, 249, and 183 mA h g^{-1} at the current densities of 0.1, 0.2, 0.5, 1, 2, 5, and 10 A g^{-1}, respectively. The capacities of bare Bi_2S_3 are 722, 493, 361, 228, 90, 22, and 14 mA h g^{-1} under the same conditions. When the current density returns to 0.1 A g^{-1}, a capacity of 619 mA h g^{-1} can be recovered for $Bi_2S_3@SiO_2$, and this capacity is much higher than that of Bi_2S_3 (237 mA h g^{-1}). The results indicate that the $Bi_2S_3@SiO_2$ has better electrochemical performances than the bare Bi_2S_3, especially at high current densities. When tested at 10 A g^{-1}, the $Bi_2S_3@SiO_2$ still delivers a capacity of 183 mA h g^{-1}, while the capacity of Bi_2S_3 decreases to less than 15 mA h g^{-1} under the same current density.

Fig. 5c displays the long-life cycling performance of $Bi_2S_3@SiO_2$ at the current density of 1 A g^{-1}. The initial and second discharge capacities are 689 and 414 mA h g^{-1}, respectively. After 1000 cycles, the discharge capacity remains at 405 mA h g^{-1}, corresponding to a capacity retention of 97.8% against the second cycle. After 4000 cy-

cles, the capacity retains at 379 mA h g^{-1}, corresponding to a capacity retention of 91.5% (an average loss of only 0.0021% per cycle). The long-life cycling performance demonstrates the outstanding cycling stability of the $Bi_2S_3@SiO_2$ microwires.

The electrochemical impedance spectroscopy (EIS) was measured to analyze the reaction kinetics of the discharge-charge process. The EIS is composed of an obvious semicircle at high frequency region and a slope line at low frequency region. The semicircle is ascribed to the charge transfer impedance. The slope line is attributed to the Warburg impedance (W_o), which indicates the diffusion of Li$^+$ in the electrode material. The inset is the equivalent circuit model, R_e, R_{ct}, and CEP represent the resistance due to the electrolyte, the charge transfer resistance through the electrode and electrolyte interface, and the constant phase element indicating the non-ideal capacitance due to the surface roughness.[36,38] The fitted data reveals that the $Bi_2S_3@SiO_2$ (76.8 Ω) exhibits similar R_{ct} value to that of Bi_2S_3 (80.7 Ω). Although the amorphous SiO_2 shell allows the Li$^+$ to pass through,[31,34] it retards the Li$^+$ diffusion to a certain degree. As a result, the $Bi_2S_3@SiO_2$ shows smaller Li$^+$ diffusivity than the bare Bi_2S_3 before cycling, as can be indicated by the slope of the inclined line in Fig. 6.

In order to understand the origin of the superior electrochemical performances of $Bi_2S_3@SiO_2$, the detailed reaction kinetics of $Bi_2S_3@SiO_2$ and Bi_2S_3 before cycling, charged to 3 V at the 1st cycle, 10th cycle, 20th cycle, and 100th cycle are investigated. It can be seen clearly that the semicircle after the 1st discharge-charge process is much smaller than that of before cycling for both $Bi_2S_3@SiO_2$ and Bi_2S_3. As the electrochemical reaction facilitates the contact
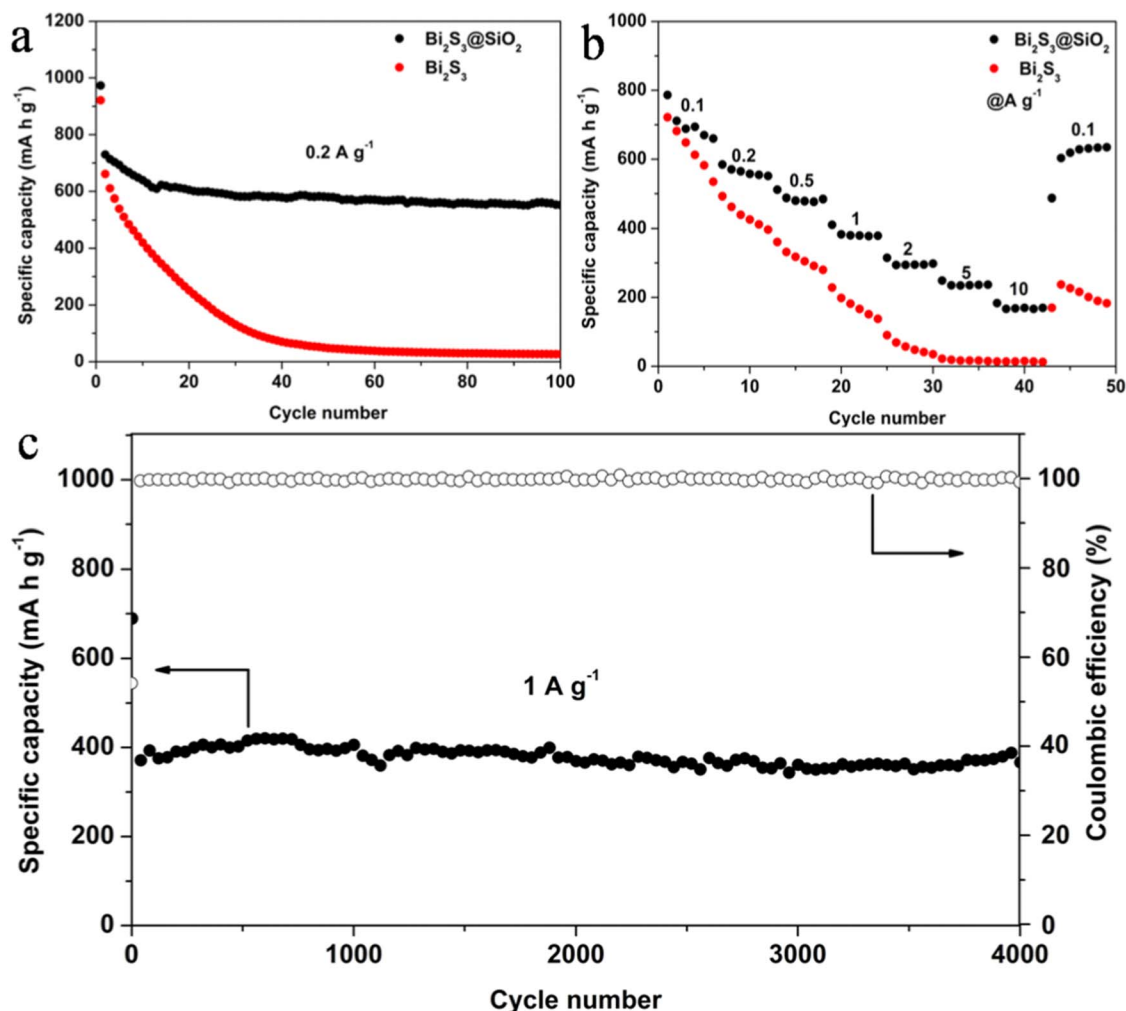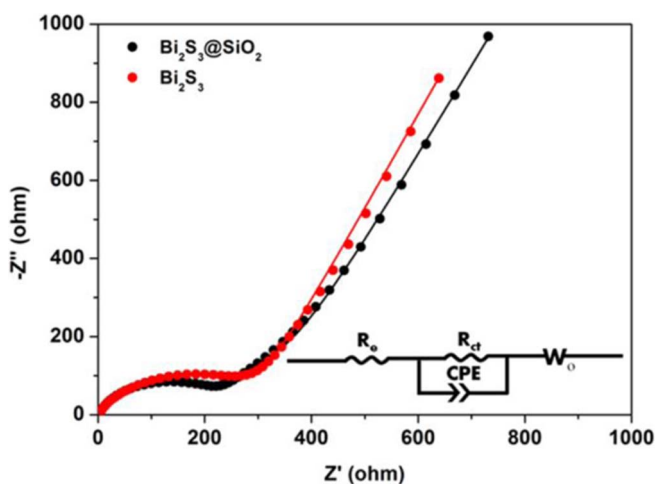
Figure 5. Cycling performances of bare Bi_2S_3 and $Bi_2S_3@SiO_2$ microwires at a current density of 0.2 A g^{-1} (a), rate performances of Bi_2S_3 and $Bi_2S_3@SiO_2$ microwires (b), cycling performance and coulombic efficiency of $Bi_2S_3@SiO_2$ microwires at a current density of 1 A g^{-1} (c).

between the electrolyte and the electrode, the interfacial impedance of the fresh electrode is reduced.[39] As shown in Fig. 7a, the diameter of the semicircle increases with cycling in the first 20 cycles due to the formation of SEI.[40,41] After 20 cycles, the charge transfer impedance


Figure 6. EIS of $Bi_2S_3@SiO_2$ and Bi_2S_3 microwires. The inset is the corresponding equivalent circuit.

of the $Bi_2S_3@SiO_2$ becomes stable and the EIS of the 100th cycle almost overlaps with that of the 20th cycle, indicating that the original morphology of $Bi_2S_3@SiO_2$ is preserved. However, the semicircle of Bi_2S_3 increases monotonously, indicating the repeated formation of SEI film and the pulverization of the Bi_2S_3 electrode. The Li$^+$ diffusivity of $Bi_2S_3@SiO_2$ doesn't change significantly with cycling (Fig. 7a), suggesting the formation of a thin and stable SEI film. In sharp contrast, the Li$^+$ diffusivity of Bi_2S_3 decreases constantly with cycling (Fig. 7b), indicating that the repeated formation and rupture of SEI film retards Li$^+$ diffusion. As a result, the Li$^+$ diffusivity in $Bi_2S_3@SiO_2$ exceeds that in bare Bi_2S_3 from the 10th cycle onward. The EIS results unambiguously demonstrate that the SiO$_2$ shell is beneficial to the formation of a thin and stable SEI film.

In order to verify the speculation, ex-situ SEM is employed to investigate the morphologies of $Bi_2S_3@SiO_2$ and Bi_2S_3 after 100 cycles at discharged state (Fig. 8). The core-shell one-dimensional microwire morphology of the $Bi_2S_3@SiO_2$ is well maintained after cycling, and no cracks can be observed (Fig. 8a). In sharp contrast, severe pulverization of the active material is observed in the case of bare Bi_2S_3. The ultralong Bi_2S_3 microwires broke into short microrods (Fig. 8b). It unambiguously demonstrates that the SiO$_2$ coating is effective to suppress the volume expansion and retain the morphology, which is beneficial for the cycling stability.
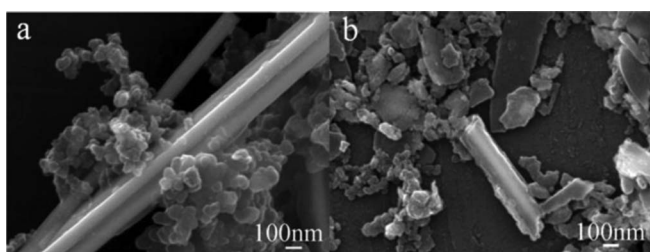
Based on the EIS and ex-situ SEM results, the superior electrochemical performance of the $Bi_2S_3@SiO_2$ microwires can be attributed to the following reasons. I) The SiO$_2$ shell constrains the
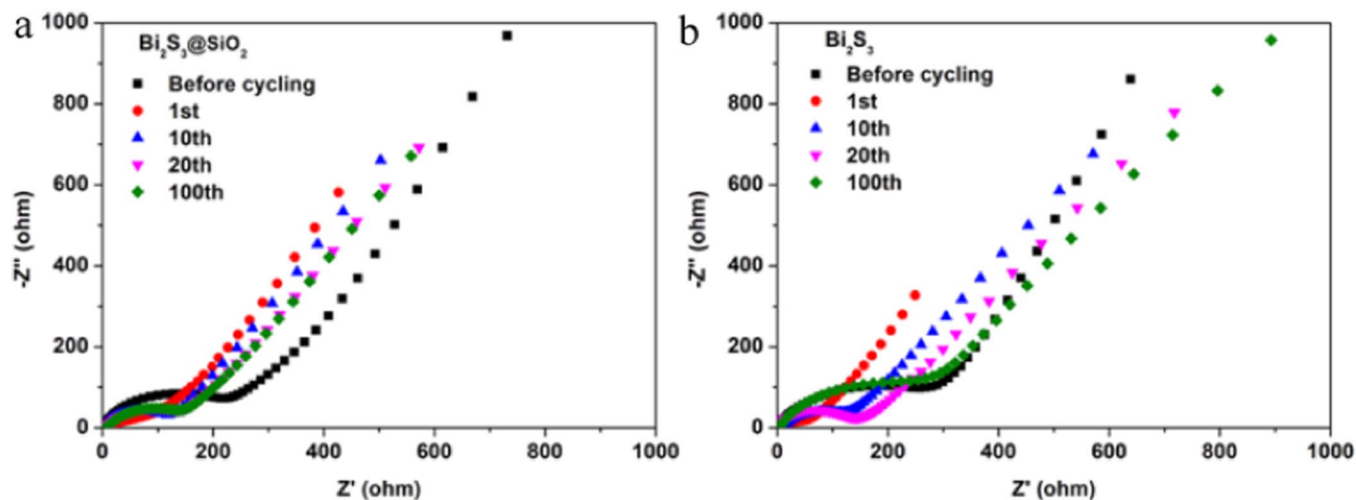
Figure 7. EIS before cycling, charged to 3 V at the 1st cycle, 10th cycle, 20th cycle, and 100th cycle for $Bi_2S_3@SiO_2$ (a), Bi_2S_3 (b).

Figure 8. SEM images of the $Bi_2S_3@SiO_2$ (a) and Bi_2S_3 (b) after 100 cycles.

volume variation of the Bi_2S_3 core and thus helps to maintain the structural integrity of the $Bi_2S_3@SiO_2$ microwires. II) The SiO_2 shell avoids the repeated formation and rupture of SEI film, playing a significant role in the thin and stable SEI formation.

Conclusions

A simple and scalable method has been developed to coat the Bi_2S_3 microwires with an amorphous SiO_2 layer. The as-obtained $Bi_2S_3@SiO_2$ composite exhibits excellent electrochemical performance with long cycle life and high capacity. The excellent electrochemical performance is ascribed to the amorphous SiO_2 coating on the Bi_2S_3 microwires, which effectively suppress the volume expansion of Bi_2S_3 and help the formation of a thin and stable SEI film.

References

1. Q. H. Xie, Y. T. Ma, X. P. Wang, D. Q. Zeng, L. S. Wang, L. Q. Mai, and D. L. Peng, *ACS Nano*, **10**, 1283 (2016).
2. L. Zhang, H. B. Wu, B. Liu, and X. W. Lou, *Energy Environ. Sci.*, **7**, 1013 (2014).
3. J. Lu, X. Y. Fan, C. F. Zhou, Z. W. Liu, F. Zheng, K. S. Lee, and L. Lu, *J. Electrochem. Soc.*, **163**, A197 (2016).
4. C. K. Chan, H. L. Peng, G. Liu, K. McIlwrath, X. F. Zhang, R. A. Huggins, and Y. Cui, *Nature Nanotech.*, **3**, 31 (2008).
5. W. M. Zhang, J. S. Hu, Y. G. Guo, S. F. Zheng, L. S. Zhong, W. G. Song, and L. J. Wan, *Adv. Mater.*, **20**, 1160 (2008).
6. P. Poizot, S. Laruelle, S. Grugeon, and J. M. Tarascon, *Nature*, **407**, 496 (2000).
7. L. W. Ji, Z. Lin, M. Alcoutlabi, and X. W. Zhang, *Energy Environ. Sci.*, **4**, 2682 (2011).
8. G. Chen, Y. Yu, K. Zheng, T. Ding, W. L. Wang, Y. Jiang, and Q. Yang, *Small*, **11**, 2848 (2015).
9. G. Konstantatos, L. Levina, J. Tang, and E. H. Sargent, *Nano Lett.*, **8**, 4002 (2008).
10. A. K. Rath, M. Bernechea, L. Martinez, and G. Konstantatos, *Adv. Mater.*, **23**, 3712 (2011).
11. D. Becerra, M. T. S. Nair, and P. K. Nair, *J. Electrochem. Soc.*, **158**, H741 (2011).
12. C. J. Tang, Y. S. Zhang, J. F. Su, C. Q. Wang, R. R. Sun, J. Zhang, and G. H. Li, *Solid State Sciences*, **51**, 24 (2016).
13. J. H. Chen, S. Y. Qin, G. X. Song, T. Y. Xiang, F. Xin, and X. H. Yin, *Dalton Trans.*, **42**, 15133 (2013).
14. Y. Fang, C. Peng, R. Guo, L. F. Zheng, J. B. Qin, B. Q. Zhou, M. W. Shen, X. W. Lu, G. X. Zhang, and X. Y. Shi, *Analyst*, **138**, 3172 (2013).
15. J. Liu, X. Zheng, L. Yan, L. Zhou, G. Tian, W. Y. Yin, L. M. Wang, Y. Liu, Z. B. Hu, Z. J. Gu, C. Y. Chen, and Y. L. Zhao, *ACS nano*, **9**, 696 (2015).
16. Q. T. Wang, X. B. Wang, W. J. Lou, and J. C. Hao, *New J. Chem.*, **34**, 1930 (2010).
17. B. Zhang, X. C. Ye, W. Y. Hou, Y. Zhao, and Y. Xie, *J. Phys. Chem. B*, **110**, 8978 (2006).
18. Y. Zhao, T. T. Liu, H. Xia, L. Zhang, J. X. Jiang, M. Shen, J. F. Ni, and L. J. Gao, *J. Mater. Chem. A*, **2**, 13854 (2014).
19. Y. Zhao, D. L. Gao, J. F. Ni, L. J. Gao1, J. Yang, and Y. Li, *Nano Research*, **7**, 765 (2014).
20. H. Jung, C. M. Park, and H. J. Sohn, *Electrochimica Acta*, **56**, 2135 (2011).
21. A. Q. Pan, H. B. Wu, L. Zhang, and X. W. Lou, *Energy Environ. Sci.*, **6**, 1476 (2013).
22. Y. Z. Luo, X. Xu, X. C. Tian, Q. L. Wei, M. Y. Yan, K. N. Zhao, X. M. Xu, and L. Q. Mai, *J. Mater. Chem. A*, **4**, 5075 (2016).
23. C. J. Tang, J. Z. Sheng, C. Xu, S. M. B. Khajehbashi, X. P. Wang, P. Hu, X. J. Wei, Q. L. Wei, L. Zhou, and L. Q. Mai, *J. Mater. Chem. A*, **3**, 19427 (2015).
24. X. J. Wei, C. J. Tang, X. P. Wang, L. Zhou, Q. L. Wei, M. Y. Yan, J. Z. Sheng, P. Hu, B. L. Wang, and L. Q. Mai, *ACS Appl. Mater. Interfaces*, **7**, 26572 (2015).
25. Z. A. Zhang, C. K. Zhou, H. Lu, M. Jia, Y. Q. Lai, and J. Li, *Mater. Lett.*, **91**, 100 (2013).
26. R. C. Jin, G. H. Li, Z. J. Zhang, L. X. Yang, and G. Chen, *Electrochimica Acta*, **173**, 458 (2015).
27. Z. A. Zhang, C. K. Zhou, L. Huang, X. W. Wang, Y. H. Qu, Y. Q. Lai, and J. Li, *Electrochimica Acta*, **114**, 88 (2013).
28. Q. Y. An, F. Y. Xiong, Q. L. Wei, J. Z. Sheng, and L. He , D. L. Ma, Y. Yao, and L. Q. Mai, *Adv. Energy Mater.*, **5**, 1401963 (2015).
29. J. F. Ni, Y. Zhao, T. T. Liu, and H. H. Zheng , L. J. Gao , C. L. Yan and L. Li, *Adv. Energy Mater.*, **4**, 1400798 (2014).
30. H. K. Song, K. T. Lee, M. G. Kim, L. F. Nazar, and J. Cho, *Adv. Funct. Mater.*, **20**, 3818 (2010).
31. S. Sim, P. Oh, S. Park, and J. Cho, *Adv. Mater.*, **25**, 4498 (2013).
32. L. W. Su, Z. Zhou, and M. M. Ren, *Chem. Commun.*, **46**, 2590 (2010).

33. K. Z. Cao, L. F. Jiao, Y. C. Liu, H. Q. Liu, Y. J. Wang, and H. T. Yuan, *Adv. Funct. Mater.*, **25**, 1082 (2015).
34. H. Wu, G. Chan, J. Wook Choi, Ill Ryu, Y. Yao, M. T. McDowell, S. W. Lee, A. Jackson, Y. Yang, L. B. Hu, and Y. Cui, *Nature Nanotech.*, **7**, 310 (2012).
35. Z. P. Liu, J. B. Liang, S. Li, S. Peng, and Y. T. Qian, *Chem. Eur. J.*, **10**, 634 (2004).
36. H. Noh and W. C. Choi, *J. Electrochem. Soc.*, **163**, A1042 (2016).
37. P. Zhan, S. A. Wang, Y. Yuan, K. L. Jiao, and S. Q. Jiao, *J. Electrochem. Soc.*, **162**, A1028 (2015).
38. Y. F. Dong, S. Li, K. N. Zhao, C. H. Han, W. Chen, B. L. Wang, L. Wang, B. A. Xu, Q. L. Wei, L. Zhang, X. Xu, and L. Q. Mai, *Energy Environ. Sci.*, **8**, 1267 (2015).
39. M. L. Li, X. Yang, C. Z. Wang, N. Chen, F. Hu, X. F. Bie, Y. J. Wei, F. Du, and G. Chen, *J. Mater. Chem. A*, **3**, 586 (2015).
40. H. X. Ji, L. L. Zhang, M. T. Pettes, H. F. Li, S. S. Chen, L. Shi, R. Piner, and R. S. Ruoff, *Nano Lett.*, **12**, 2446 (2012).
41. Y. Z. Luo, X. Xu, X. C. Tian, Q. L. Wei, M. Y. Yan, K. N. Zhao, X. M. Xu, and L. Q. Mai, *ACS Appl. Mater. Interfaces*, **8**, 2812 (2016).